Assessment of Power Quality in Low Voltage Networks Considering Uncertainty in Harmonics Generated by Photovoltaic Inverters using Monte Carlo

BRYAN ISAÍAS JIMÉNEZ POMA[1], LUIS ROLANDO CRUZ PANCHI[1],
CARLOS IVÁN QUINATOA CAIZA[2]
[1]Cotopaxi Technical University,
ECUADOR

[2]Universidad Técnica de Cotopaxi,
ECUADOR

Abstract: - The massive integration of photovoltaic systems into low-voltage grids introduces power quality challenges due to harmonic distortion. This article presents a probabilistic assessment using Monte Carlo simulation based on experimental measurements taken over seven consecutive days of three commercial inverter technologies, yielding 5,168,640 data points with one-minute resolution. The results reveal a 34-fold disparity in total harmonic distortion (THD): pure sine wave inverters exhibit 1.00% ± 0.20%, complying with IEEE 519-2014, while square-wave and modified-wave inverters exhibit 30.10% ± 2.10% and 34.60% ± 4.30%, exceeding regulatory limits. Through 10,000 simulations on the CIGRE European LV Benchmark network, it is demonstrated that nodes with high-quality inverters have a zero probability of violation, while low-quality inverters have a probability exceeding 97%. For a 9.7% PV penetration rate, the probability of violation reaches 8.5%. Penetration limits of 7.5% are established, or the proportion of high-quality inverters should be increased to 85–100%.

Key-Words: - Power quality, Total harmonic distortion, Photovoltaic inverters, Monte Carlo simulation, probabilistic analysis, Distributed generation, Low-voltage networks.

Received: March 11, 2026. Revised: May 13, 2026. Accepted: June 10, 2026. Published: July 20, 2026.

1 Introduction

The growing penetration of photovoltaic (PV) systems into low-voltage distribution networks has heightened concerns about the quality of the electrical power delivered to end users, [1]. Globally, installed solar power capacity exceeded 1 TW in 2022 [2], driven by a reduction in the cost of photovoltaic modules by more than 90% over the past decade, [3]. It is worth noting that solar energy capacity by the end of 2024 was 2.2 TW, [4]. In the Latin American context, and specifically in Ecuador, this deployment has been characterized by the simultaneous use of different commercial inverter technologies, whose electrical performance varies substantially, [5].

The photovoltaic inverter is the critical interface and the primary source of harmonic distortion in these systems [6] its impact depends on the switching method: pure sine wave (PWM) inverters typically keep the THD below 3% through high-frequency filtering, [7]. In contrast, square-wave and modified-wave inverters [8], widely used due to their lower cost in residential and rural installations, generate low-order harmonics (3rd, 5th, and 7th) that exceed 30%, surpassing the 5% limit established by the IEEE 519-2014 standard, [8]. Recent field studies in low-voltage networks indicate that the presence of low-quality inverters raises the total harmonic distortion (THD) of the voltage to levels outside the standard under high irradiance conditions, [8]. Due to propagation through line impedances [9], this distortion affects even adjacent nodes that do not have faulty inverters, [10]. Conventional deterministic analyses evaluate fixed scenarios [11], ignoring variability due to solar irradiance, the type and magnitude of the connected load, [12]. Previous studies have documented that these approaches can underestimate the actual probability of regulatory violations by up to 40% [13], representing an unquantified risk for the planning and operation of grids with high photovoltaic penetration, [14]. The lack of experimental validation regarding the variability of commercial inverters under diverse loads [15] is critical in markets such as Ecuador's, where the diversity of manufacturing standards and the lack of field verification of local regulations (ARCERNNR 003/23) necessitate specific quality requirements.

1.1 Contributions

In contrast to previous studies that model irradiance variability but treat the harmonic behavior of the inverter as a fixed or deterministic value [16], [17], this study incorporates, for the Ecuadorian market, the inherent uncertainty of the THD of three commercial technologies simultaneously within a Monte Carlo simulation framework on a standardized reference grid. In particular, the work in [17], which performs a comparative analysis of power quality among the same three waveforms (sinusoidal, square, and modified) under static conditions, differs from the present study in the following respects: (i) the generation of a new database of 5,168,640 records with one-minute resolution, (ii) the probabilistic modeling of THD variability using fitted distributions, and (iii) the propagation of this uncertainty via Monte Carlo simulation on the CIGRE European LV Benchmark network, quantifying the probabilities of regulatory violations.

1.2 Objective of the Study

The objective of this study is to probabilistically quantify the impact of harmonic uncertainty generated by different commercial photovoltaic inverter technologies on power quality in low-voltage networks, by integrating experimental characterization, statistical modeling, and Monte Carlo simulation in the CIGRE European LV Benchmark test network. The following specific objectives are proposed: (1) to experimentally characterize the harmonic behavior of three commercial inverter technologies pure sine wave, square wave, and modified sine wave under controlled load and irradiance conditions; (2) to fit probability distribution models calibrated to the experimental records; (3) to quantify, through 10,000 Monte Carlo simulations, the probability of non-compliance with the IEEE 519-2014 standard at each network node; and (4) to determine the photovoltaic penetration thresholds for regulatory compliance, [18].

Finally, the content of the article is described: Section 2 presents the problem formulation, describing the mathematical model used; Section 3 describes the solution to the problem, as well as future work; and Section 4 presents the conclusions.

2 Statement of the Problem

2.1 Harmonic Generation by Inverter Technology

Photovoltaic inverters can be classified into three categories based on their topology, [6]. Pure sine wave inverters use PWM modulation (>20 kHz) and LC filtering at the output to achieve a voltage THD typically below 3%, which is compatible with the limits established by IEEE 519-2014. Variability in THD is associated with changes in the operating point of the maximum power point tracking (MPPT) algorithm, [19]. The output signal of a square-wave inverter is represented by the Fourier series shown in (1), where V_p is the peak amplitude f_0 is the fundamental frequency, and n is the odd harmonic order. This expression shows that the signal contains only odd harmonics.

$$v(t) = \frac{4V_p}{\pi} \sum_{n=1,3,5,\ldots} \frac{1}{n} \sin(2\pi n f_0 t) \tag{1}$$

This implies theoretical values of H3 = 33.3%, H5 = 20%, and H7 = 14.3% relative to the fundamental frequency, resulting in THD values exceeding 25%, [20]. Modified-wave inverters use intermediate-level switching but retain the 3rd, 5th, and 7th harmonics as dominant components, with reported THD values between 25% and 45%, [21]. These types exhibit greater variability (CV of up to 15%) than the square wave, due to the sensitivity of their modulation pattern to load changes.

2.2 Modeling Inverters as Harmonic Current Sources

For propagation analysis, the inverter is represented by the harmonic Norton model, a current source in parallel with its internal impedance, [11]. Its validity in low-voltage networks stems from the fact that the system impedance is considerably lower at the inverter output. The mathematical representation associates with each inverter k a set of harmonic currents $\{I_{h,k}\}$ proportional to its fundamental current:

$$I_{h,k} = I_{1,k} \cdot \frac{H_{h,k}}{100} \tag{2}$$

where $H_{h,k}$ is the percentage of the hth harmonic relative to the fundamental, obtained from measurements or statistical models [10]. The main limitation of this approach is that it treats the harmonics from different inverters as independent of one another, ignoring possible phase-synchronization effects. Therefore, this assumption may influence the estimation of the aggregate harmonic impact, potentially leading to a slight underestimation or overestimation. Harmonic propagation is governed by equations (3) and (4), which imply that higher-order harmonics encounter greater inductive impedance, [21].

$$\mathrm{V}_h = \mathrm{Z}_h \mathrm{I}_h \tag{3}$$

$$\mathrm{Z}(h) = \mathrm{R} + jh\mathrm{X} \tag{4}$$

2.3 Probabilistic Approaches to Power Quality Assessment

The stochastic nature of photovoltaic generation and the variability in inverter behavior make deterministic analyses insufficient for quantifying the actual risk of non-compliance with standards. This limitation has led to the development of probabilistic methodologies that explicitly incorporate uncertainty in system parameters, [22]. Critical sources of uncertainty include solar irradiance, typically modeled using Beta distributions due to their suitability for bounded variables [23], and variability in the electrical characteristics of inverters, for which truncated normal distributions have shown good fit in experimental studies, [21]. Monte Carlo simulation is the gold standard method for propagating these uncertainties through the network model and obtaining complete distributions of power quality variables, [24]. By dispensing with assumptions about linearity or the shape of distributions, it outperforms analytical methods in scenarios with asymmetric inputs or nonlinear models, [25], as illustrated in Figure 1.

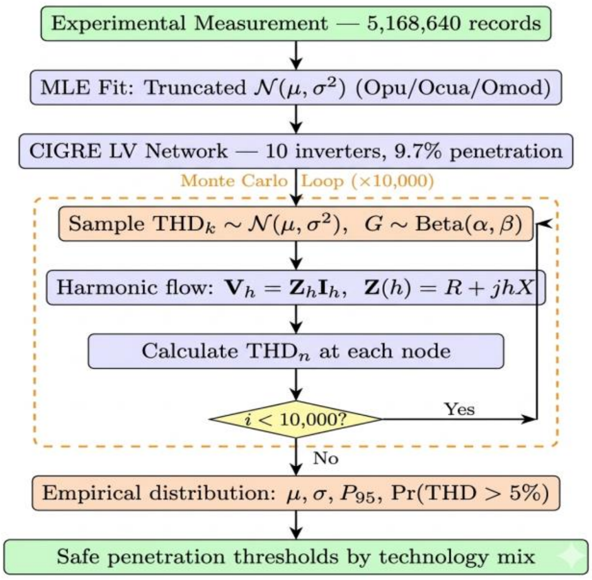

Fig. 1: Flowchart of the proposed methodology
Source: created by the authors.

Based on a systematic review of more than 90 recent articles, it was determined that Monte Carlo simulation is the most widely used tool for the stochastic analysis of distributed generation networks, [9]. Improved variants such as Latin hypercube sampling (LHS), quasi-Monte Carlo, and importance sampling offer superior computational efficiency with very similar results, [23]. Previous studies have applied this type of simulation to evaluate the impact of distributed generation on power quality [26], but most consider only the variability of irradiance [16] omitting the dispersion in the harmonic behavior of the inverters themselves, [17].

The classical Monte Carlo method was selected due to its robustness and ease of implementation for probabilistic harmonic analysis. Although variance reduction techniques such as Latin Hypercube Sampling (LHS) could improve computational efficiency, the standard approach was considered sufficient for the purposes of this study. The Monte Carlo method was implemented with N = 10,000 simulations. Convergence was evaluated based on the stability of the mean voltage THD value at the system nodes, with variations of less than 1% observed as the number of simulations increased, indicating convergence of the results.

2.4 Characterization of Photovoltaic Inverters

Characterization is the central pillar of this work; the data were obtained using a Fluke 1777 measuring instrument. This section describes the experimental design, the equipment used, the load scenarios evaluated, the resulting database, and the statistical fitting that converts the measurements into harmonic source models. The measurements were performed on a test module designed and built at the Technical University of Cotopaxi, following the experimental procedure documented in [18].

Three technologies representative of the Ecuadorian market were selected: Opu (pure sine wave), based on PWM modulation at over 20 kHz with LC filtering, offering higher harmonic quality; Ocua (square wave), direct switching at grid frequency without filtering, low-cost, but with high harmonic content; and Omod (modified wave), a stepped waveform at moderate frequency. Each inverter was subjected to five load conditions: (1) no load (<0.1 A), to characterize the intrinsic THD; (2) very low load (0.06–0.25 A), purely resistive; (3) medium load (0.25–1.5 A), resistive-inductive, representative of household appliances; (4) high load (1.5–3.0 A), multiple nonlinear loads in parallel; and finally (5) pure resistive load, a bank of calibrated resistors to isolate the inverter's harmonic contribution.

The measurement process yielded a database of 5,168,640 records with one-minute resolution, distributed across 1,472 parameters per column, as shown in Table 1, where v_i and I_i are voltage and effective currents, $THD_i$is the total harmonic distortion of voltage, $H_{n,i}$ are the individual harmonics expressed as a percentage of the fundamental, c_i is the load condition, and t_i is the duration of the record, as defined in (5).

$$\mathrm{D}_i = \{V_i, I_i, \mathrm{THD}_i, H_{3,i}, H_{5,i}, H_{7,i}, H_{9,i}, H_{11,i}, C_i, t_i\} \quad (5)$$

Table 1. Distribution of the experimental dataset (7 days and 1 minute resolution)

Investor Type	Records	Porcentage (%)
Pure wave (Opu)	1.693.440	32.8
Square wave (Ocua)	1.612.800	31.2
Modified wave (Omod)	1.814.400	35.1
Three phase network (ref.)	47.999	0.9
Total	**5.168.640**	**100**

Source: created by the authors.

2.4.1 Overall THD Statistics

Table 2 summarizes the statistical parameters of the THD measured for each technology. The disparity among the types is the most significant finding: Opu inverters have an average THD of 1.00%, while Ocua and Omod reach 30.10% and 34.60%, respectively a difference of up to 34 times. All three types comply with the voltage level requirement of regulation ARCERNNR 003/23, but only Opu meets the 5% THD limit established by [8].

Table 2. THD statistical parameters by inverter type.

Type	μ (%)	σ (%)	Min. (%)	Max. (%)	CV (%)	n
Opu	1.00	0.20	0.8	1.4	20.0	21
Ocua	30.10	2.10	27.9	33.7	7.0	20
Omod	34.60	4.30	27.9	41.4	12.4	24

CV: Coefficient of variation = $\sigma/\mu \times 100\%$}
Source: created by the authors.

2.4.2 Load Scenarios and THD Dependency

Spectrum analysis reveals qualitative differences between technologies that justify treating them differently in the network model. For Opu inverters, harmonics H3 through H11 together account for 1.08% of the fundamental frequency, with no single harmonic exceeding 0.5%. For Ocua and Omod, harmonics H3, H5, and H7 account for between 60% and 85% of the total THD, confirming the theoretical square-wave pattern described in Table 3.

Table 3. Average Individual Harmonics by Inverter Type (% of Fundamental).

Type	H3	H5	H7	H9	H11
Opu	0.28	0.31	0.24	0.15	0.10
Ocua	14.2	15.8	10.1	5.80	3.20
Omod	16.0	17.0	12.5	6.50	4.00

Source: created by the authors.

The Pearson correlation between load and THD varies depending on the technology: Opu ($r = -0.68$) and Omod ($r = -0.72$)reduce their THD as the load increases[14]; conversely $Ocua$ ($r = -0.15$) exhibits structural distortion independent of the load.

2.4.3 Statistical Fitting and Probabilistic Models

Four families of distributions were evaluated: Normal, Log-Normal, Gamma, and Weibull using maximum likelihood, with goodness-of-fit verified using the following complementary statistical tests: Kolmogorov-Smirnov (K-S), Anderson-Darling (A-D), Shapiro-Wilk (S-W), and Jarque-Bera (J-B). The truncated Normal distribution performed best, with p-values greater than 0.80 in all tests, as shown in Table 4.

Table 4. Results of Goodness of Fit Tests (p-values).

Type	K-S	A-D	S-W	J-B
Opu	0.91	0.88	0.85	0.83
Ocua	0.87	0.84	0.82	0.80
Omod	0.89	0.86	0.83	0.81

Source: created by the authors.

The probabilistic models that represent each technology as a source of variable harmonic current are shown in equations (6) - (8). These calibrated models serve as the direct input to the simulation block described in the following section. The Opu model captures its moderate operational variability (CV=20%), while the Ocua and Omod models reflect distributions that are more concentrated around high THD values, with CVs of 7.0% and 12.4%, respectively.

$$THDOpu \sim \mathcal{N}(1.00, 0.20^2)\ trunc.en\ [0.8, 1.4] \quad (6)$$

$$\mathrm{THD_{Ocua}} \sim \mathcal{N}(30.1, 2.10^2)\mathrm{trunc.\ en}\ [27.9, 33.7]\% \quad (7)$$

$$\mathrm{THD_{Omod}} \sim \mathcal{N}(34.6, 4.30^2)\mathrm{trunc.\ en}\ [27.9, 41.4]\% \quad (8)$$

The experimentally obtained harmonic distortion levels for each inverter technology exhibit variability around a central value due to operating conditions such as load changes, as well as switching behavior. This variability is approximated by a truncated normal distribution, as it allows for the representation of the concentration of values around the mean. Alternative distributions such as Weibull or Gamma were considered to represent the variability of THD; however, the normal distribution showed a better fit according to goodness of fit tests ($\boldsymbol{K-S, A-D, S-W}$).

2.5 Grid Integration and Harmonic Flow

This section describes the test network, the location of the inverters, the harmonic flow model implemented, and the metrics used to quantify the impact on power quality. Monte Carlo simulation is used to estimate the probability distributions. Figure 2 shows the distribution of nodal THD obtained after 10,000 Monte Carlo iterations. Furthermore, it is observed that nodes with Opu inverters concentrate their values in the 0.8–1.4% range, while nodes with Ocua and Omod inverters show distributions shifted toward 10–20%, as indicated by the disparity reported in Table 2. The positive skew of these latter distribution values justifies the use of the P95 percentile instead of the mean value.

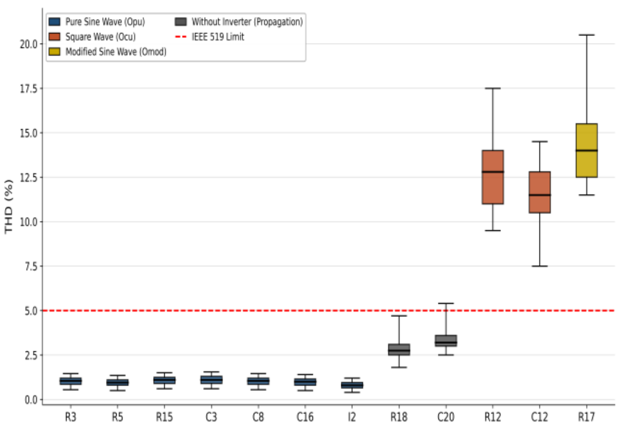

Fig. 2: Distribution of the nodal THD obtained using 10,000 Monte Carlo

Source: created by the authors.

2.5.1 CIGRE European LV Benchmark Test Network

The European low-voltage test network developed by CIGRE Task Force C6.04, which is widely used in studies on the integration of distributed energy resources, was adopted, [27]. This network models a 400 V three-phase system with a grounded neutral (3F+N configuration) and comprises three feeders with characteristics representative of real-world environments:

- Residential Feeder (R): 19 nodes, 17 sections, total length 0.57 km.
- Commercial Feeder (C): 21 nodes, 20 sections, total length 0.60 km.
- Industrial Feeder (I): 3 nodes, 1 section, length 0.20 km.

Each feeder is served by a Dyn1 transformer (20/0.4 kV) with a short-circuit impedance of 4%, with rated capacities of 500 kVA (residential), 300 kVA (commercial), and 150 kVA (industrial). The network uses six types of standard conductors, three overhead (OH1–OH3) and three undergrounds (UG1–UG3), with cross-sections ranging from 16 mm² to 240 mm². The load distribution is summarized in Table 5**.**

Table 5. Load Distribution in the CIGRE

Feeder	P (kW)	Q (kVAr)	FP
Residential	383.8	126.2	0.95
Industrial	85.0	44.7	0.85
Commercial	217.8	105.4	0.90
Total	**686.6**	**284.3**	**0.924**

Source: created by the authors.

2.5.2 Location and Integration of PV Inverters

Ten inverters were connected across the three feeders, resulting in a PV penetration rate of 9.7% relative to total demand. The technology mix adopted (7 Opu, 2 Ocua, 1 Omod) reflects a realistic market distribution in which high-quality inverters predominate but coexist with lower-quality units. The configuration is detailed in Table 6. The selection of nodes follows the criterion of representing electrically diverse locations: nodes near the transformer (R3, C3), intermediate nodes (R12, C12), and remote nodes (R17, C16).

Table 6. Configuration of PV Inverters in the Grid.

Node	Type	P $_{nom}$ (kW)	Feeder
R3	Opu	5.0	Residential
R5	Opu	3.0	Residential
R12	Ocua	4.0	Residential
R15	Opu	6.0	Residential
R17	Omod	3.5	Residential
C3	Opu	10.0	Commercial
C8	Opu	8.0	Commercial
C12	Ocua	5.0	Commercial
C16	Opu	7.0	Commercial
I2	Opu	15.0	Industrial
Total		**66.5**	

Source: created by the authors.

2.5.3 Harmonic Flow Model

Each inverter is represented as a harmonic current source of order h according to equation (9). Where $H_{h,k}$ is sampled at each iteration of the simulation based on the distributions given by equations (6), (7), and (8). Furthermore, P_k scales with the irradiance according to equation (10). Harmonics up to the 17th order ($H_{máx} = 17$), were considered, covering 99.5% of the experimental harmonic behavior. The harmonic flux follows the matrix framework of the classical load flux extended to multiple frequencies [11], for each order h, the nodal admittance matrix $Y^{(h)} \in \mathbb{C}^{n\times n}$ with elements $Y_{ij}^{(h)} = \frac{1}{Z_{ij}^{(h)}}$, where $Z_{ij}^{(h)} = R_{ij} + jhX_{ij}$ is the frequency impedance of branch ij.

The vector of nodal harmonic voltages $V^{(h)} \in \mathbb{C}^n$ is obtained by solving the system $\mathrm{V}_h = \mathrm{Z}_h \mathrm{I}_h$ or its equivalent $\mathrm{Z}_h = \mathrm{Y}_h^{-1}$ established in Equation (11). Using Kron's reduction to the neutral conductor [28], the phase matrices z_{abc} are obtained, enabling the unbalanced three-phase analysis of the CIGRE network (3F+N configuration).

$$I_{h,k} = I_{1,k} \cdot \frac{H_{h,k}}{100}, I_{1,k} = \frac{P_k}{\sqrt{3}V_{LL}\cos\phi_k} \quad (9)$$

$$P_k = P_{\mathrm{nom},k} \cdot \frac{G}{G_{\mathrm{STC}}}, G \sim \mathrm{Beta}(\alpha = 2, \beta = 5) \times 1200\mathrm{W/m}^2 \quad (10)$$

$$\mathrm{V}_h = \mathrm{Z}_h \mathrm{I}_h, \qquad \mathrm{Z}_h = \mathrm{Y}_h^{-1} \quad (11)$$

2.5.4 Power Quality Metrics

The voltage THD is calculated at each node n. Based on $N_{sim} = 10{,}000$Monte Carlo iterations (N_o = 10,000), which is selected by convergence of the standard error of the violation probability as described in (12), ensuring an accuracy of ±0.6% with 95% confidence; it should be noted that tests with N = 5,000 and N = 20, 000 confirmed differences of less than 0.4%), in this context, the complete empirical distribution of THD_n, is obtained for each node, from which the mean μ_{THD} and standard deviation σ_{THD} the percentiles P_5, P_{50}, and P_{95}, and the probability of violating the IEEE 519-2014 limit are extracted.

$$p \approx 0.09\mathrm{y}\sqrt{\frac{p(1-p)}{N}} \approx 0.003 \quad (12)$$

$$\mathrm{THD}_n = \frac{\sqrt{\sum_{h=2}^{H_{max}} |V_{h,n}|^2}}{|V_{1,n}|} \times 100\% \quad (13)$$

$$Pr(\mathrm{THD} > 5\%) = \frac{1}{N_{\mathrm{sim}}} \sum_{i=1}^{N_{\mathrm{sim}}} \mathbb{1}(\mathrm{THD}_{n,i} > 5\% \quad (14)$$

$$F_n(x) = \frac{1}{N} \sum \mathbf{1}(\mathrm{THD}_i \le x) \quad (15)$$

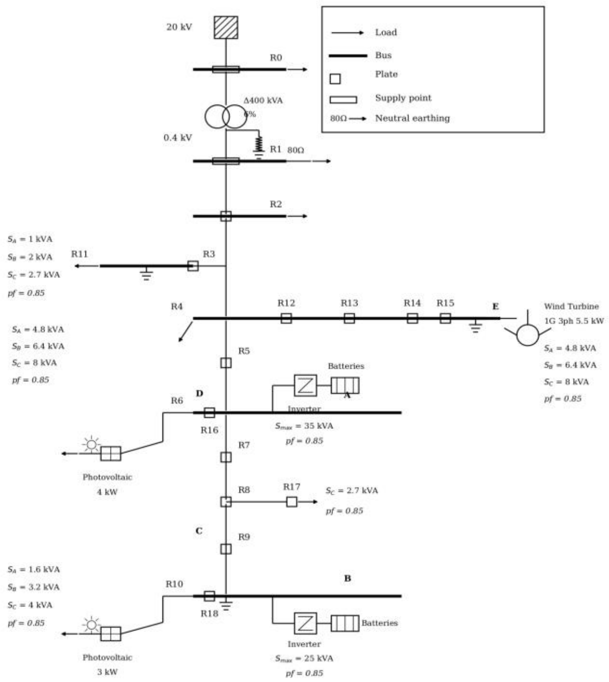

Fig. 3: Single-line diagram of the CIGRE European LV Benchmark network with integrated PV inverters

Source: created by the authors.

The P_{95} percentile is particularly important from a regulatory standpoint: a node that satisfies P_{95} <

5% ensures that it operates within the limit 95% of the time, which is a more stringent and realistic condition than simply verifying the mean value. The single-line diagram of the modeled system is shown in Figure 3.

3 Solution to the Problem

The results of the 10,000 Monte Carlo simulations on the CIGRE network provide an answer to the central question of this study: To what extent does the choice of inverter technology affect the harmonic quality of the grid, both at the connection node and through propagation effects. Table 7 presents the THD statistics at the nodes where inverters are connected. The difference between technologies is immediate and striking.

Table 7. Nodal THD at Inverter Connection Points

Node	**Type**	μ (%)	σ (%)	**P95** (%)	**Pr(THD >5%)**
R3	Opu	0.95	0.18	1.26	0.00
R5	Opu	0.88	0.16	1.17	0.00
R15	Opu	1.02	0.19	1.34	0.00
C3	Opu	1.12	0.21	1.48	0.00
C8	Opu	1.05	0.20	1.38	0.00
C16	Opu	0.98	0.18	1.29	0.00
I2	Opu	0.82	0.15	1.08	0.00
R12	Ocua	12.80	2.42	16.90	98.5
C12	Ocua	11.50	2.15	15.20	97.8
R17	Omod	14.20	3.18	19.50	99.2

Source: created by the authors.

Nodes with Opu inverters maintain an average THD below 1.2% in all cases, with zero probability of exceeding the 5% limit set by IEEE 519-2014, [8]. The margin of compliance is ample even at the P_{95} percentile, which does not exceed 1.5% in any Opu node. This confirms that this technology poses no harmonic risk under any combination of irradiance and load within the experimental range. The contrast with the Ocua and Omod nodes is stark. Nodes R12 and C12 exhibit average THDs of 12.8% and 11.5%, with violation probabilities of 98.5% and 97.8%, respectively. Node R17 (Omod) achieves the highest average THD in the system, 14.2%, with a P_9s of 19.5% and a violation probability of 99.2%. The greater dispersion of node R17 compared to R12 and C12 (σ = 3.18% vs. 2.42%) is consistent with the higher coefficient of variation of the Omod inverter (CV = 12.4%) compared to the Ocua inverter (CV = 7.0%).

3.1 Remote Impact: Harmonic Propagation in the Grid

A particularly significant finding is that the influence of the Ocua and Omod inverters is not limited to their connection nodes, but propagates to adjacent nodes that do not have faulty inverters. Table 8 quantifies this effect at nodes without their own inverters.

Table 8. Nodal THD at Nodes without an Inverter: Propagation Effect

Node	μ (%)	σ (%)	**P95** (%)	**Pr(THD>5%)**
R0 (slack)	0.42	0.08	0.56	0.00
R18 (remote)	2.85	0.68	4.05	0.12
C20 (remote)	3.42	0.82	4.88	0.68

Source: created by the authors.

The attenuation pattern with distance is quantified by analyzing the average THD as a function of the electrical distance to the node with the faulty inverter. The attenuation is approximately 10–15% per 30 meters, consistent with the increase in inductive impedance for low-order harmonics described by $Z(h) = R + j^hX$. For the 3rd harmonic: $Z_3 \approx 1.03\Omega/\text{km}$; for the 5th harmonic $Z_5 \approx 1.58\Omega/\text{km}$; for the 7th $Z_7 \approx 2.16\Omega/\text{km}$. No significant resonances were identified in the 3rd–17th harmonic range for the CIGRE network. The maximum amplification factor observed was 1.08, attributable to the moderate length of the network (< 1.4 km) and the absence of capacitive compensation, [21].

3.2 Sensitivity: Technology as the Dominant Factor

Sensitivity analysis using the Morris method allows for the quantification of the relative contribution of each source of uncertainty to the resulting nodal THD. The results, expressed by the index μ^*, which is the average of the absolute values of the elementary effects described in (16) and (17).

$$EE_i = \frac{f(x + \Delta \cdot e_i) - f(x)}{\Delta} \quad (16)$$

$$\mu^* = \frac{1}{r}\sum|EE_i| \quad (17)$$

Furthermore, Table 9 clearly shows that inverter technology is the dominant factor in grid THD, both due to its intrinsic distortion ($\boldsymbol{\mu}^*$ = 0.685) and its proportion in the mix ($\boldsymbol{\mu}^*$= 0.524). Solar irradiance has a moderate impact ($\boldsymbol{\mu}^*$= 0.312) while line impedance is marginal ($\boldsymbol{\mu}^*$= 0.092). This confirms that harmonic quality must be ensured at the generation stage, as the grid does not provide sufficient attenuation.

Table 9. Morris Sensitivity Indices for Nodal THD

Uncertainty factor	$\boldsymbol{\mu}^*$	**Range of influence**
THD of Ocua/Omod inverters	0.685	Dominant
Ocua/Omod proportion in the mix	0.524	High
Solar irradiance	0.312	Moderate
Line impedance	0.092	Marginal

Source: created by the authors.

3.3 Penetration Thresholds and Technology Mix

Table 10 shows the evolution of the average grid THD, as well as the probability of regulatory violations as a function of the level of photovoltaic penetration, maintaining the constant technological combination of the base scenario (70% Opu, 20% Ocua, 10% Omod).

Table 10. Impact of PV Penetration Level on Harmonic Quality

Penetration	**THD Average**	**Pr(THD> 5%)**	**Nodes in**	**Nodes**
(%)	**(%)**	**(%)**	**violation**	**critical**
0	0.38	0.0	0	0
5	1.82	2.1	2	0
9.7	3.15	8.5	3	1
15	4.68	22.8	5	2
20	6.25	45.2	8	4

Source: created by the authors.

The critical threshold lies between 7% and 8% penetration for the current mix: below this value, the probability of a breach remains below 5% at all nodes; above it, at least one node consistently exceeds the regulatory limit. With a mix of 85% Opu and 15% Ocua, the safe penetration threshold rises to 12–13%, while with 100% Opu, the probability of a violation is zero for any penetration level within the evaluated range. Conversely, with the current Ocua/Omod ratio increased to 40%, the threshold falls below 5%, making even low penetration levels a regulatory risk. These results are summarized in Table11.

Table 11. Penetration and Technological Mix Thresholds

Inverter mix	**Safe Threshold (%)**	**Pr(THD>5%) at 9.7%**
100% Opu	>20	0.0
85% Opu + 15% Ocua	12-13	3.2
70% Opu + 20% Ocua		
+ 10% Omod (base)	7-8	8.5
60% Opu + 40% Ocua/Omod	<5	31.4

Source: created by the authors.

Taken together, the results in this section demonstrate that inverter technology is not a secondary design parameter: it is the variable that determines whether a grid with moderate photovoltaic penetration operates within or outside regulatory limits, both at connection nodes and at adjacent nodes affected by harmonic propagation.

Figure 4 illustrates the nonlinear behavior of the probability of nodes in violation: between 0% and 5% penetration, the increase is moderate (0 to 2.1%), but between 9.7% and 20%, the curve accelerates significantly (from 8.5% to 45.2%). This pattern confirms the existence of a critical threshold around 7.5% penetration, below which the system operates with a low probability of non-compliance; therefore, if the system operates above this threshold, the regulatory risk increases sharply.

The switching topology determines harmonic behavior: PWM inverters (Opu) operate at 20–50 kHz and filter their high-frequency harmonics, achieving a THD of 1.0%, while square-wave and modified-square-wave inverters inject low-order harmonics (H3, H5, H7) with little attenuation, reaching 30.1% and 34.6% with a 34-fold disparity [29]. The differentiated coefficients of variation (CV: 20% Opu, 7.0% Ocua, 12.4% Omod) confirm that square-wave distortion is structural and invariant, which prevents compliance with the 5% limit under any operating condition. The absence of resonances in the 3rd–17th order range is due to the network length (< 1.4 km) and the lack of capacitors, a result that cannot be generalized to networks with long cables or capacitor banks, [21].

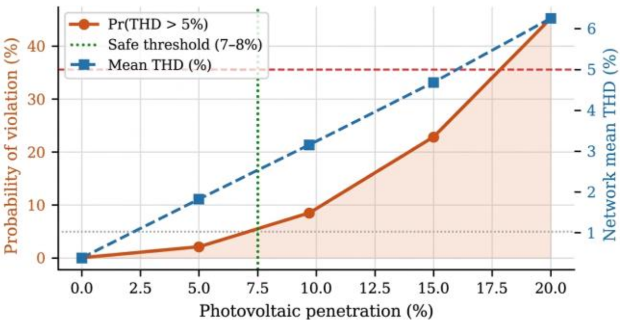

Fig. 4: Impact of PV penetration level on average THD and the probability of violation
Source: created by the authors.

3.4 Comparison with the Literature and Implications for Networks.

The results are consistent with previous studies [21], which report THD values of 1–3% for PWM inverters and 25–35% for modified sine wave inverters, encompassing the values obtained (1.0% and 34.6%) [25], finds violation probabilities of 5–12% for penetration levels of 10–15%, consistent with the 8.5% obtained at 9.7% penetration; attenuation of 12–18% over 25–30 m, slightly higher than the 10–15% observed, attributable to the specific conductors of the CIGRE network. Compared to the 3–5% reported in the literature [30], the THD of 1.0% obtained is attributed to variability among manufacturers and measurement methodologies. The main contribution is the dataset of 5,168,640 data points (7 days with 1-minute resolution) statistically validated through four tests, [18], surpassing standard point measurements, [31]. By integrating statistical models and harmonic flow for the three technologies simultaneously. For the CIGRE network with the current mix, the threshold is 7.5%; with 100% Opu, this threshold exceeds 20%.

3.4.1 Limitations and Scope of the Results

The results of this study are limited by the experimental conditions and the network model used. The measurements were performed on commercial inverters available on the Ecuadorian market under controlled conditions, without accounting for the effects of aging or extreme temperatures. The CIGRE network represents a moderate-length European system without capacitive compensation; therefore, the propagation results, as well as the absence of resonances, cannot be directly extrapolated to other networks.

3.5 Future Projects

Future research directions include: (1) characterization of interactions among multiple synchronized inverters; (2) time-series analysis accounting for daily/seasonal variability; (3) modeling of nonlinear loads and harmonic interactions; (4) extension to interharmonics and superharmonics (> 2 kHz); (5) development of adaptive controllers for real-time active mitigation; and (6) experimental validation in operational grids under real world conditions.

4 Conclusions

The characterization of 5,168,640 records over seven consecutive days reveals a 34-fold disparity in average THD among the inverters: the Opu inverters at 1.00% ± 0.20% also comply with the IEEE 519-2014 standard with a margin of 2.80%, while Ocua 30.10% ± 2.10% and Omod 34.60% ± 4.30%, exceeding the regulatory limit of 5%.

Sensitivity analysis using the Morris method identifies the intrinsic THD of the Ocua/Omod inverters ($\boldsymbol{\mu}^*$= 0.685) and their proportion in the mix ($\boldsymbol{\mu}^*$= 0.524) as the factors with the greatest influence on the nodal THD, that is, solar irradiance has a moderate influence (μ^*= 0.312), while line impedance is marginal (μ^*= 0.092).

With the base case mix (70% Opu, 20% Ocua, 10% Omod), in this context, photovoltaic penetration must be limited to 7.5% to keep the probability of violation nodes below 5% and with a 95th percentile as the evaluation criterion, rather than the mean value or the deterministic worst-case scenario.

References:

[1] F. Blaabjerg, R. Teodorescu, M. Liserre, y A. Timbus, “Overview of control and grid synchronization for distributed power generation systems”, IEEE Transactions on Industrial Electronics, vol. 53, núm. 5, pp. 1398–1409, oct. 2006, doi: 10.1109/TIE.2006.881997.

[2] International Energy Agency, “Renewables 2022 - Analysis and forecast to 2027”, 2022.

[3] International Renewable Energy Agency, “Renewable power generation costs in 2021”, 2022.

[4] J. Gorączkowska, M. Moczulska, y S. Yatsunenko, “TESE-Informed Evolution Pathways for Photovoltaic Systems: Bridging Technology Trajectories and

Market Needs", Energies (Basel)., vol. 18, núm. 23, p. 6216, dic. 2025, doi: 10.3390/en18236216.

[5] M. Mahmud, H. Pota, y M. Hossain, "Nonlinear current control scheme for a single-phase grid-connected photovoltaic system", IEEE Trans. Sustain. Energy, vol. 5, núm. 1, pp. 218–227, ene. 2014, doi: 10.1109/TSTE.2013.2279884.

[6] S. Kjaer, J. Pedersen, y F. Blaabjerg, "A review of single-phase grid-connected inverters for photovoltaic modules", IEEE Trans. Ind. Appl., vol. 41, núm. 5, pp. 1292–1306, sep. 2005, doi: 10.1109/TIA.2005.853371.

[7] G. Chicco, J. Schlabbach, y F. Spertino, "Experimental assessment of the waveform distortion in grid-connected photovoltaic installations", Solar Energy, vol. 83, núm. 7, pp. 1026–1039, jul. 2009, doi: 10.1016/j.solener.2009.01.005.

[8] IEEE Std 519-2014, "IEEE Recommended Practice and Requirements for Harmonic Control in Electric Power Systems", mar. 2014, doi: 10.1109/IEEESTD.2014.6826459.

[9] T. P. Abud, A. A. Augusto, M. Z. Fortes, R. S. Maciel, y B. Borba, "State of the Art Monte Carlo Method Applied to Power System Analysis with Distributed Generation", Energies 2023, Vol. 16, Page 394, vol. 16, núm. 1, p. 394, dic. 2022, doi: 10.3390/en16010394.

[10] J. H. R. Enslin y P. J. M. Heskes, "Harmonic-interaction between a large number of distributed power inverters and the distribution network", IEEE Trans. Power Electron., vol. 19, núm. 6, pp. 1586–1593, nov. 2004, doi: 10.1109/TPEL.2004.836615.

[11] J. Arrillaga y N. R. Watson, Power System Harmonics. John Wiley & Sons, 2004.

[12] G. Chicco, J. Schlabbach, y F. Spertino, "Experimental assessment of the waveform distortion in grid-connected photovoltaic installations", Solar Energy, vol. 83, núm. 7, pp. 1026–1039, jul. 2009, doi: 10.1016/j.solener.2009.01.005.

[13] Y. B. Lee, R. Mitten, K. C. Liu, y G. A. Seyfert, "The China Light And Power Company Energy Management System", IEEE Transactions on Power Systems, vol. 6, núm. 1, pp. 199–205, 1991, doi: 10.1109/59.131063.

[14] IEEE, IEEE Standard for Interconnection and Interoperability of Distributed Energy Resources with Associated Electric Power Systems Interfaces. IEEE, 2018.

[15] A. Yazdani y R. Iravani, Voltage-sourced converters in power systems : modeling, control, and applications. IEEE Press/John Wiley, 2010.

[16] Y. Wang, N. Zhang, Z. Zhenyu, C. Kang, y D. Kirschen, "Mixed-integer linear programming-based optimal configuration planning for energy hub: Starting from scratch", Appl. Energy, vol. 210, pp. 1141–1150, ene. 2018, doi: 10.1016/j.apenergy.2017.08.114.

[17] T. P. Abud, R. S. Maciel, y B. S. M. C. Borba, "Improved Monte Carlo techniques for distributed generation impact evaluation", Electrical Engineering, vol. 106, núm. 6, pp. 7167–7179, dic. 2024, doi: 10.1007/s00202-024-02336-5.

[18] E. D. Albán, K.F. Basantes, y E. D. Guamán, "Comparative Analysis of Power Quality in Square-Wave, Modified Sine-Wave, and Pure Sine-Wave Inverters in Off-Grid", 2025.

[19] O. Penangsang, R. S. Wibowo, N. K. Aryani, M. D. Prasetyo, M. N. Arianto, y A. A. LutfI, "Harmonic assessment on two photovoltaic inverter modes and mathematical models on low voltage network power quality", International Journal of Electrical and Computer Engineering, vol. 13, núm. 6, pp. 5951–5965, dic. 2023, doi: 10.11591/ijece.v13i6.pp5951-5965.

[20] S. K. Rangu, P. R. Lolla, K. R. Dhenuvakonda, y A. R. Singh, "Recent trends in power management strategies for optimal operation of distributed energy resources in microgrids: A comprehensive review", Int. J. Energy Res., vol. 44, núm. 13, pp. 9889–9911, oct. 2020, doi: 10.1002/er.5649.

[21] R. Langella, A. Testa, J. Meyer, F. Moller, R. Stiegler, y S. Z. Djokic, "Experimental-Based Evaluation of PV Inverter Harmonic and Interharmonic Distortion Due to Different Operating Conditions", IEEE Trans. Instrum. Meas., vol. 65, núm. 10, pp. 2221–2233, oct. 2016, doi: 10.1109/TIM.2016.2554378.

[22] G. Carpinelli, D. Lauria, y P. Varilone, "Voltage stability analysis in unbalanced power systems by optimal power flow", IEE Proceedings - Generation, Transmission and

Distribution, vol. 153, núm. 3, pp. 261–268, 2006, doi: 10.1049/ip-gtd:20050011.

[23] I. C. Barutcu, G. Sharma, R. V. Gandhi, V. K. Jadoun, y A. Garg, "Investigations on solar PV integration and associated power quality challenges in distribution systems through the application of MCS and GA", Journal of Engineering and Applied Science, vol. 71, núm. 1, dic. 2024, doi: 10.1186/s44147-024-00449-z.

[24] R. Y. Rubinstein y D. P. Kroese, Simulation and the Monte Carlo Method: Third Edition. wiley, 2016. doi: 10.1002/9781118631980.

[25] K. Sundareswaran, S. Peddapati, y S. Palani, "MPPT of PV systems under partial shaded conditions through a colony of flashing fireflies", IEEE Transactions on Energy Conversion, vol. 29, núm. 2, pp. 463–472, 2014, doi: 10.1109/TEC.2014.2298237.

[26] F. J. Ruiz-Rodríguez, J. C. Hernández, y F. Jurado, "Probabilistic Load-Flow Analysis of Biomass-Fuelled Gas Engines with Electrical Vehicles in Distribution Systems", Energies 2017, Vol. 10, Page 1536, vol. 10, núm. 10, p. 1536, oct. 2017, doi: 10.3390/en10101536.

[27] E. Mulenga, M. H. J. Bollen, y N. Etherden, "A review of hosting capacity quantification methods for photovoltaics in low-voltage distribution grids", International Journal of Electrical Power & Energy Systems, vol. 115, p. 105445, feb. 2020, doi: 10.1016/j.ijepes.2019.105445.

[28] W. H. Kersting, "Distribution system modeling and analysis, Third Edition", p. 432, 2012.

[29] J. Guo y Y. Li, "An agent mechanism for sharing users' integrated energy considering contribution rate", Sustainable Energy, Grids and Networks, vol. 26, p. 100457, jun. 2021, doi: 10.1016/j.segan.2021.100457.

[30] S. Markkassery, A. D. Mahindrakar, N. Lakshminarasamma, y R. Pasumarthy, "Modelling of non-isolated single-input-multi-output DC-DC converter", IEEE International Conference on Power Electronics, Drives and Energy Systems, jul. 2018, doi: 10.1109/PEDES.2018.8707836.

[31] International Electrotechnical Commission, Electromagnetic compatibility (EMC) - Part 4-30: Testing and measurement techniques - Power quality measurement methods. IEC 61000-4-30:2025: International Electrotechnical Commission, 2015.

Contribution of Individual Authors to the Creation of a Scientific Article (Ghostwriting Policy)

The authors equally contributed in the present research, at all stages from the formulation of the problem to the final findings and solution.

Sources of Funding for Research Presented in a Scientific Article or Scientific Article Itself

No funding was received for conducting this study.

Conflict of Interest

The authors have no conflicts of interest to declare that are relevant to the content of this article.